5-1984

Patterns of Earthquakes and the Effect of Solid Earth and Ocean Load Tides at Mount St. Helens Prior to the May 18, 1980, Eruption

Stephen R. McNutt
Columbia University, smcnutt@usf.edu

R. J. Beavan
University of Washington

JOURNAL OF GEOPHYSICAL RESEARCH, VOL. 89, NO. B5, PAGES 3075-3086, MAY 10, 1984

PATTERNS OF EARTHQUAKES AND THE EFFECT OF SOLID EARTH AND OCEAN LOAD TIDES AT MOUNT ST. HELENS PRIOR TO THE MAY 18, 1980, ERUPTION

S. R. McNutt[1],[2] and R. J. Beavan

Lamont-Doherty Geological Observatory of Columbia University

Abstract. Seismographs near Mount St. Helens Volcano recorded an earthquake swarm lasting nearly 2 months prior to the catastrophic May 18, 1980, eruption. The earthquakes are divided into four classes based on station CPW (Δ = 116 km) seismogram characteristics: (1) events with Sv:P amplitude ratio >3 and dominant frequency >3 Hz; (2) events with Sv:P ratio between 1 and 3 and dominant frequency >2 Hz; (3) events similar to characteristic 2 but with a strong (probably surface wave) phase just after the S phase; and (4) events with frequencies between 1 and 2 Hz lacking a clear S phase. The seismicity pattern for each of the four classes is unique, and we assume each group of events with similar waveforms represents a common physical process, depth, source area, or fault orientation. Maximum likelihood b values range between 0.97 ± 0.05 and 1.81 ± 0.09 for the four groups. We calculate solid earth stress and strain tides at the average hypocentral depth of 4 km. We also calculate stress and strain tides induced by ocean loading; their amplitudes are typically 20-40% those of the solid earth tides at the location of Mount St. Helens. A weak but significant correlation exists between the latter two classes of events and the tides for a time interval of about 5 days preceding the first onset of volcanic tremor and about 5 days thereafter. The polarity of the correlation is opposite for the two classes of events. In each case, the phase of the correlation changes systematically with time, the changes coinciding with the onset of tremor on March 31 and with a pronounced decrease in earthquake energy release rate on April 3. There are no significant correlations between the tides and the number of events or energy release of these two classes of earthquakes during any other interval between March 20 and May 18, 1980. The first two classes of events show no evidence of significant tidal correlation at any time during the study period.

Introduction

At the time of the 1980 Mount St. Helens eruptions, there was extensive speculation in the media and scientific circles whether any correlation existed between the eruptions and earth or ocean tides.

Volcanic earthquakes at Pavlof Volcano, Alaska, correlated well with the solid earth tide for a few days immediately preceding and immediately following explosive eruptions [McNutt and Beavan, 1981]. The development through time of a correlation between volcanic earthquakes and tides therefore had potential as an eruption predictor at Pavlof Volcano. In this study we examine the volcanic earthquakes and tidal data at Mount St. Helens during the time interval between March 20, 1980, and the cataclysmic eruption of May 18, 1980. Several small eruptions took place within this time window, and more than 4000 volcanic earthquakes and periods of volcanic tremor were recorded. The earthquakes had magnitudes up to 5.1 M_L and were of several distinct classes, which we distinguish by seismogram characteristics.

For two classes of earthquakes, which we designate high- and medium-frequency (see below), we find no significant correlation between the tides and either rate of occurrence or rate of energy release of earthquakes at any time between March 20 and May 18, 1980. However, for the mixed- and low-frequency events a weak but statistically significant correlation is found between tides and both rate of occurrence and rate of energy release of earthquakes between March 27 and April 5, 1980, but not during any other time period. During this time window two observations suggest changes in the preeruptive state of the volcano. Volcanic tremor was first observed on March 31, and the cumulative energy release rate of all earthquakes decreased on April 3, 1980. At these times the phase of the correlation changes systematically, suggesting that differences in the rate or orientation of stress buildup may have occurred as magma was injected into the volcanic pile at shallow depths.

Seismicity

The catastrophic eruption of Mount St. Helens on May 18, 1980, was preceded by an earthquake swarm of approximately 2 months duration. The seismicity was studied by Endo et al. [1981], and we summarize their results below. Seismicity began to increase on March 15, 1980, as recorded by station SHW, located 4 km from the volcano's summit (Figure 1). On March 20 a magnitude 4.2 earthquake occurred 4 km beneath the mountain. This event was followed by a moderate number of low magnitude earthquakes, then on March 23 seismicity increased from 2-3 earthquakes per hour to an average of over 15 per hour (Figures 2a, 2b). A second magnitude 4 earthquake occurred on March 24, and on March 25 the seismicity increased abruptly, coinciding with a tenfold increase in the average seismic background noise level. Seismicity was highest on March 26, the day before the first steam explosion, when it reached 38 events with magnitudes greater than 2.5 in 6 hours (Figure 3). Seismicity gradually declined

[1]Also at Department of Geological Sciences, Columbia University.

[2]In cooperation with the Geophysics Program, University of Washington.

Paper number 4B0193.
0148-0227/84/004B-0193$05.00

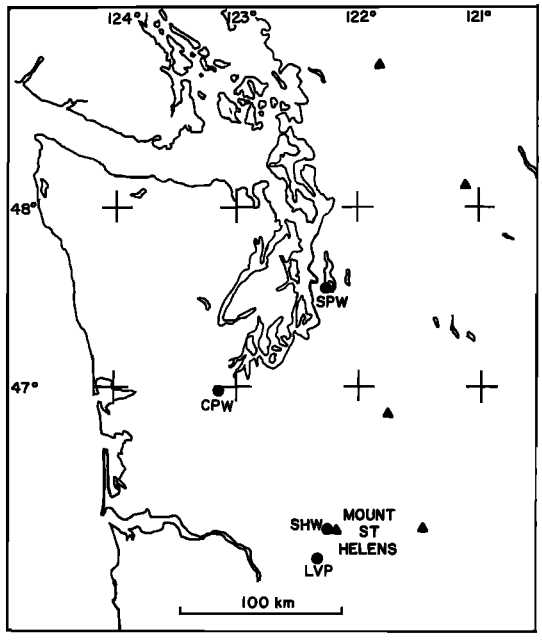

Fig. 1. Map showing locations of seismic stations (circles) and volcanos (triangles) in western Washington.

over the next several weeks to a level of about 10 events with magnitude greater than 2.5 per 6 hours (Figure 3). During this time the seismic energy release rate was roughly constant, or decreasing less rapidly than the seismicity, indicating an increase in the average magnitude of events with time. Most events had preliminary locations about 2 km north of the summit at a depth of about 4 km.

Our study uses helicorder records from station CPW (a telemetered 1-Hz vertical seismometer [Noson and Crosson, 1980]) located 116 km NW of the volcano. These records began on March 26 and ran continuously until after May 18, providing clear seismograms with low background noise. The detection threshold varied from about M_L = 1.8 to M_L = 3.0, depending on the class of events. During the study period approximately 100 min of recording time were lost at CPW during daily record changing, and other stations, particularly LVP (Figure 1), were examined during these times. An additional 145 min of recording time was lost when larger earthquakes occurred and clipped the instrument, obscuring any smaller events.

Event Classes

The events are divided into four classes based on CPW seismogram characteristics (Figure 4). All four classes appear during the first few days of CPW records, although their rates of occurrence change independently. Differences between the seismograms of the various event classes are very clear, hence we divide the seismicity into separate groups whose activity patterns and possible correlation with tidal stresses can be examined separately. The classes are as follows:

1. High-frequency events; these have clear P and S arrivals, both with frequency content >3 Hz. The Sv:P amplitude ratios are 3:1 or greater (e.g., 4:1), suggesting that station CPW may be near a P wave node. S-P times are about 14.5 s.

2. Medium-frequency events; these have clear P and S phases with frequency content >2 Hz and <3 Hz. Sv:P ratios range between 1:1 and 3:1. S-P times are about 14.5 s.

3. Mixed-frequency events; these have a strong arrival, probably a surface wave, 16.5-17 s after the P wave. Sv:P ratios are approximately 1:1. Both P and S waves have frequencies ≈2 Hz. However, the P wave is impulsive and in general has a higher frequency content than the S wave, which is often indistinct.

4. Low-frequency events; these have an emergent P wave and no clear S wave. Frequency content is nearly monochromatic between 1 and 2 Hz. They also have unusually long coda durations compared to other events of similar signal amplitude.

From March 26 to May 18, a total of 4770 events were counted on the CPW records (Table 1). Magnitudes for the large events were assigned by using M_L values published in the PDE catalogs of March, April, and May 1980; events were also spot checked and compared with Wood-Anderson records from Seattle (SPW, Figure 1). Magnitudes for the smaller events were assigned by using the coda duration versus magnitude relations of Endo et al. [1981]. We assigned magnitudes to the high- and medium-frequency events by using Endo et al.'s [1981] high-frequency event relation and to the mixed-

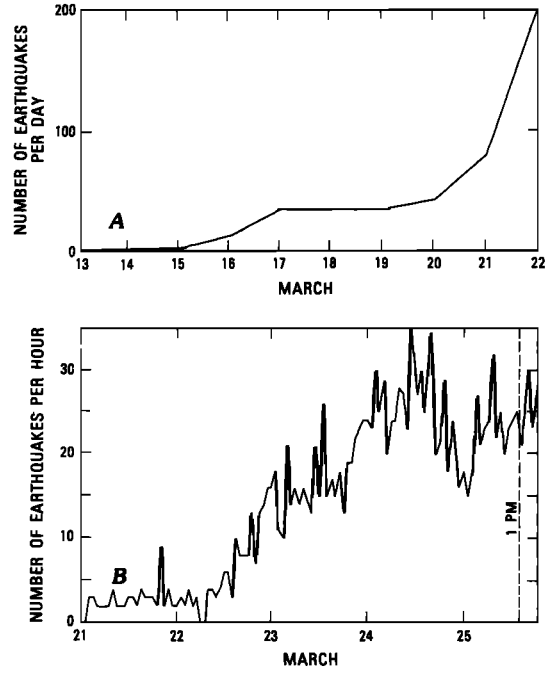

Fig. 2. Counts of earthquakes from SHW records in universal time. (a) Daily counts from March 13 to 21, 1980. Most events were of insufficient magnitude to be detected by next nearest seismic station, 50 km from the volcano. (b) Hourly counts from March 21 to midday on March 25, at which time individual events could no longer be recognized on Helicorder records [after Endo et al., 1981].

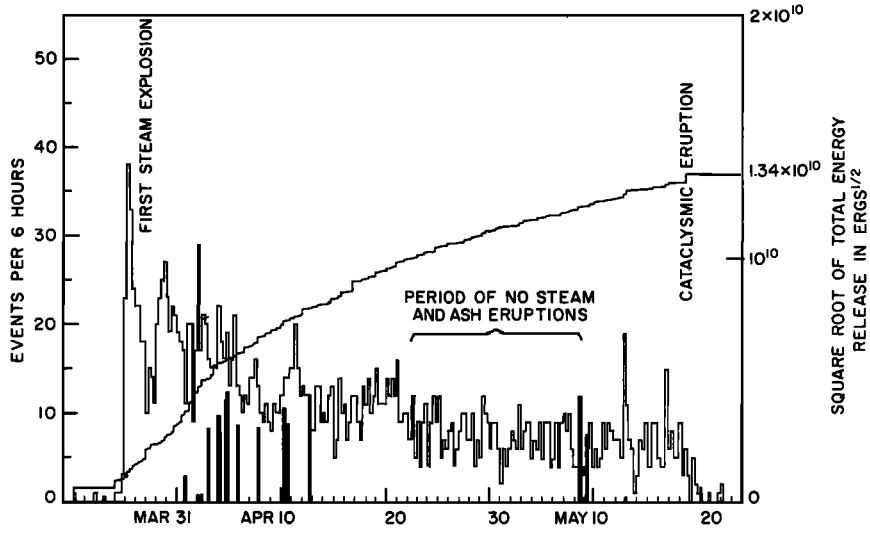

Fig. 3. Counts of earthquakes larger than magnitude 2.5 per 6 hours, volcanic tremor (vertical lines, length proportional to tremor duration), and square root of cumulative energy release from March 20 to May 24, 1980, UTC. The plot emphasizes the significant increase in large-magnitude earthquakes after the first eruption on March 27, as indicated by increase of energy release. Square root of total energy release, as of May 24, was 1.34×10^{10} ergs$^{1/2}$ [after Endo et al., 1981; Malone et al., 1981; Geophysics Program, University of Washington, 1980].

and low-frequency events based on their low-frequency event relation. The data compilation consists of counting the number of events per hour in each class for different amplitude ranges. Helicorder records, which have equally spaced traces, are particularly convenient for this purpose; counting of events is fast and would be easy to perform in real time during future eruption sequences if it were found that changes in earthquake rate or earthquake-tide correlation could be used to help predict eruptions. The choices of class and the counts were done blind, that is, without any prior knowledge of the tides. We count the events with waveforms which cross 0, 1, 2, 3, 4, or 5 adjacent helicorder traces, corresponding to peak-to-peak amplitudes of 5, 10, 15, 20, 25, and 30 mm. We then determine the average coda duration for events of each class in each amplitude range, and assign magnitudes by using the relationships of Endo et al. [1981]. The range, or error, in magnitude determinations is ±0.3. Some of the larger clipped events are difficult to assign to an event class with confidence.

We infer that events with common waveforms represent either a common physical process, a common geometry, a common depth, a restricted source area, or possibly all four. The high-frequency events correspond closely to Minakami's [1960] A-type events; the medium-frequency events would also fit this classification. The low-frequency events resemble Minakami's B-type events, except that they tend to be larger and deeper than typical low-frequency or B-type events observed at other volcanos [Endo et al., 1981]. The mixed-frequency events do not fit Minakami's classification scheme. They are gradational between the low-frequency and medium-frequency events and may represent either a combination of source processes or a propagation effect observed only at the particular station CPW. The particular set of diagnostics chosen for the classification of the Mount St. Helens seismicity is based specifically on station CPW seismograms; other stations at different distances and azimuths might require different diagnostics (e.g., frequency content, Sv:P amplitude ratios, etc.) to classify the same events into the same categories.

Statistics and Seismic Energies

Two time series were generated for each of the four classes of earthquakes. The first is the total number of events of each type per hour (Figure 5b). Because the smaller events are more numerous, these time series accentuate the smaller events. Secondly, we assign energies to the events by using Richter's [1958] relation

$$\log_{10} E = 9.9 + 1.9\, M_L - 0.024\, M_L^2$$

where E is energy in ergs and M_L is local magnitude. These time series accentuate the larger events (Figure 5c). During hours when no earthquakes occurred ($\log_{10} 0$ is unbounded), it is necessary to add a background level as an estimate of the energy released in small events not detected at CPW. We chose this to be 2 orders of magnitude less than the energy of the smallest detected events in each class; this is consistent with estimated magnitude versus frequency of occurrence relations. The b slopes of Gutenberg and Richter's [1954] relation

$$\log_{10} N = a - bM$$

where N is number of earthquakes of magnitude M or greater, and a and b are constants, were determined for each class of earthquakes by using the maximum likelihood method of Utsu [1965] (Table 1). Generally, values of 1.0 or less are associated with aftershock sequences of tectonic events [Page, 1968], and higher values, up to 2

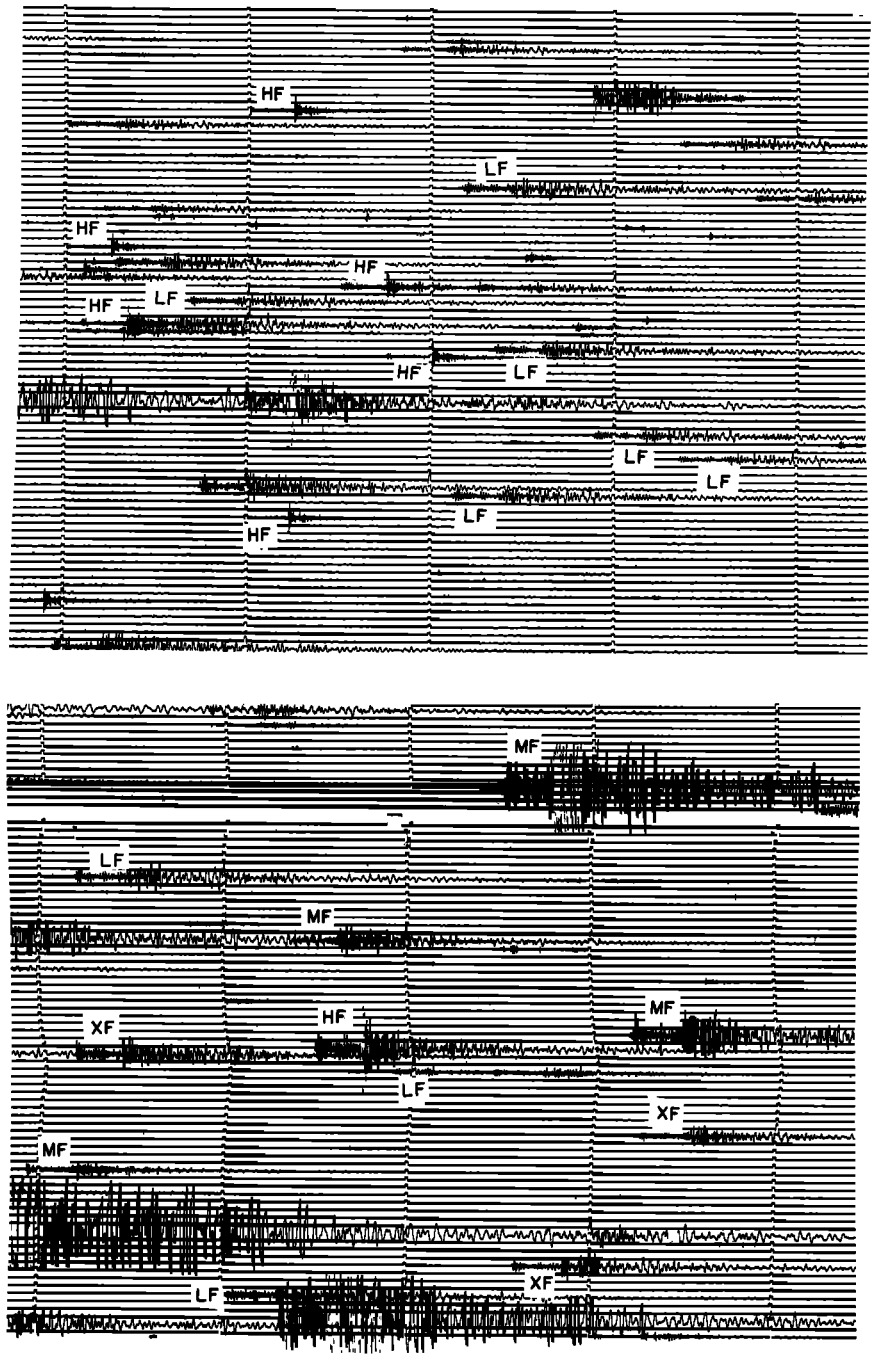

Fig. 4. Samples of CPW seismograms from (top) April 5-6 and (bottom) April 22-23. HF, high frequency; MF, medium frequency; XF, mixed frequency; LF, low frequency. Tick marks are 1 min apart.

or more, are found for volcanic events [Minakami, 1960]. The resulting b slopes differ from the values of 0.6 for high-frequency events and 2.77 for low-frequency events given by Endo et al. [1981]. We believe the present determinations differ mainly because of the use of maximum likelihood rather than linear regression for determining the b slope, but the values may also be influenced by the different classification schemes. A preliminary study by McNutt [1981] also showed some b slope nonlinearity and variation with time; however, a detailed study of these effects requires further revision of the magnitudes and clarification of the classification scheme.

Patterns of Seismicity

On the basis of results from Pavlof Volcano [McNutt and Beavan, 1981], we searched for patterns in seismicity or eruptive activity of Mount St. Helens which may have indicated a change in magmatic processes. The earlier work indicated that volcanic seismicity did not occur

TABLE 1. Number of Events in Each Class, Magnitude Thresholds, and b Values

Event Class	Magnitude Threshold	Total Number of Events	b Value
High frequency	1.8	1199	0.97 ± 0.05
Medium frequency	2.2	1416	1.81 ± 0.09
Mixed frequency	3.0	750	1.17 ± 0.08
Low frequency	3.0	1405	1.81 ± 0.09

randomly in time, but correlated systematically with tides during time periods of about 4 days prior to and after explosive eruption sequences, when magma was presumably moving at shallow levels in the crust. Several time periods of possible changes in magmatic activity at Mount St. Helens were examined for tidal correlations. The first period is the drastic increase in seismicity from March 15 to March 26. A second period is the decrease in seismicity following the first steam explosions on March 27 and lasting until about April 12 (Figure 3). A third period is the appearance of volcanic tremor on March 31; tremor continued almost daily until April 12 (Figure 3) [Malone et al., 1981]. During these tremor episodes, on about April 3, the slope of the square root of cumulative energy release curve decreased rather suddenly (Figure 3) [Endo et al., 1981]. These episodes were of low amplitude (<2 mm) and did not affect detection capability. Also, at about the same time (March 31) the bulging of the north flank of the

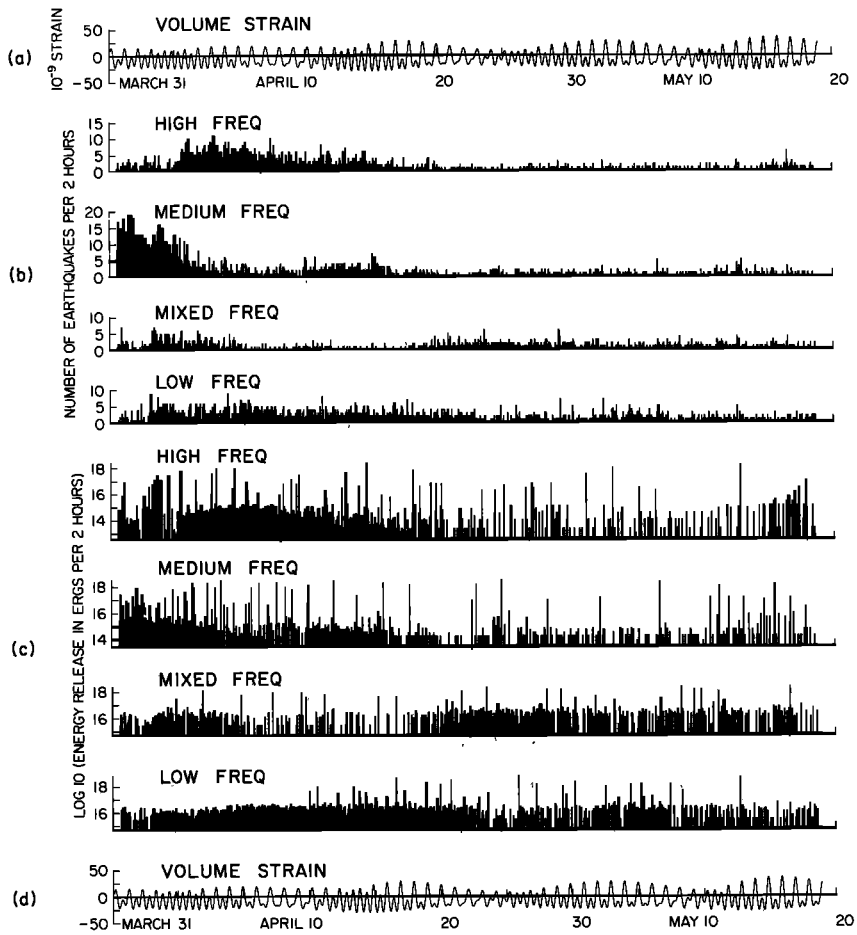

Fig. 5. (a) Theoretical volume strain tide including solid earth and ocean loading effects. (b) Number of events per 2 hours for each of the four event classes. Events were counted per hour, and the tidal correlation calculations used the hourly counts; the plot is drawn with 2-hourly counts for greater clarity. (c) Log_{10} (energy release) per 2 hours for each of the event classes. (d) Repeat of Figure 5a as an aid in visually examining the series for tidal correlations. Note that tick marks occur at the beginning (UT) of the labeled day.

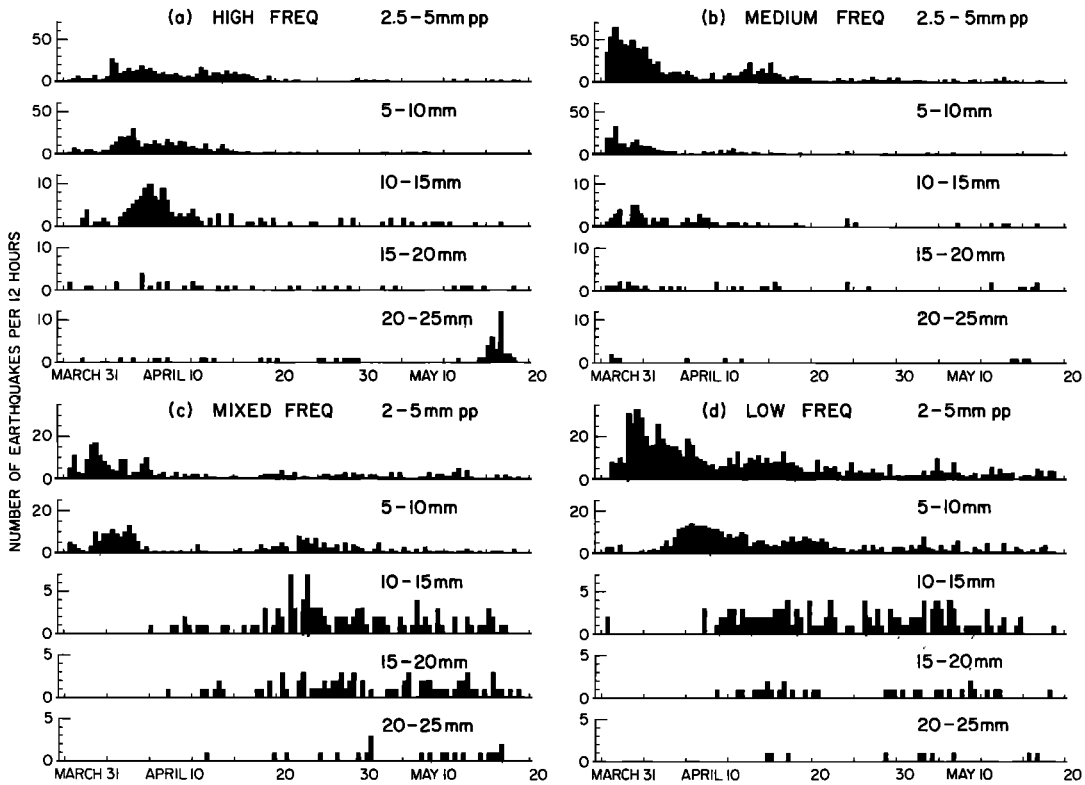

Fig. 6. Patterns of occurrence of the various classes of earthquakes: (a) number of high-frequency events per 12 hours for different size ranges (peak-to-peak amplitude in millimeters); (b) medium-frequency events; (c) mixed-frequency events; (d) low-frequency events. Note the changes in vertical scale. Tick marks occur at the beginning (UT) of the labeled day.

mountain was first documented [Krimmel and Post, 1981], although the bulging may have begun as early as March 27 [Lipman et al., 1981]. Fourth, a period of no steam and ash eruptions lasted from April 22 until May 8 [Geophysics Program, University of Washington, 1980]. The volcanic tremor on May 8 and 9 (Figure 3) [Malone et al., 1981] may have been related to the renewal of steam and ash eruptions. Last was the catastrophic eruption of May 18, accompanied by spasmodic tremor, and the rapid decline in seismicity following the major eruption episode.

The four event classes of the present study have patterns of seismicity which differ from each other and also differ from the plots of seismicity given by Malone et al. [1981], Endo et al. [1981] (Figure 3), and Geophysics Program, University of Washington [1980]. The class of medium-frequency events have their highest rate of occurrence initially (March 26-27), then the rate decays with time in a manner similar to many observed aftershock sequences (Figures 5b and 6b). Most of the smaller events recorded on station SHW between March 20 and March 26 probably belong to this event class, although seismogram characteristics are different from those on station CPW. The high-frequency events reach their maximum rate of occurrence on March 31, about the same time as the first observation of volcanic tremor. Their rate of occurrence remains high during the 13 days on which tremor is recorded, then decays (Figures 5b and 6a). The rate of occurrence of the high-frequency events increases somewhat on May 16, 2 days before the catastrophic eruption (Figures 5b and 6a). However, a few of these latter events have seismograms differing somewhat in coda shape from the vast majority of high-frequency events; these may result from differences in source processes, geometry, fault area, or depth.

The mixed- and low-frequency events have similar patterns of occurrence (Figures 5b, 6c, and 6d). Seismicity is highest during early April, but the decay in the number of events per hour is much less than for either the high- or medium-frequency events. Also, while the overall number of events per unit time decreases, the average magnitude increases so that the energy release rate remains roughly constant. This pattern is particularly striking for the low-frequency events (Figure 6d). The smallest events reach their peak rate of occurrence first. When their rate begins to decrease, the next larger size reaches their peak rate, and so on. The larger events do not appear at all until late in the sequence. Since the low-frequency events are those most peculiar to volcanos, we feel further study of this pattern may be important in terms of forecasting eruptions.

Tidal Correlations

Because the majority of the earthquakes are centered at about 4 km depth beneath the volcano [Endo et al., 1981; Decker and Decker, 1981], the tides are calculated at this depth. The solid

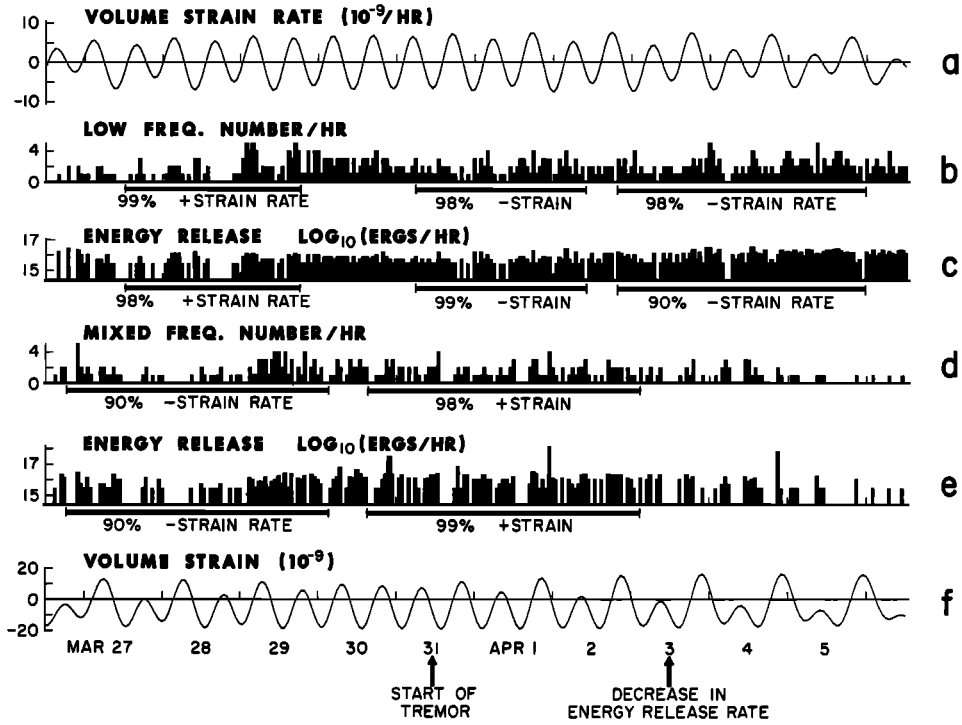

Fig. 7. Time series between March 26 and April 6, 1980, for (a) volume strain rate tide, (b) number of low-frequency events per hour, (c) $\log_{10}$ energy release of low-frequency events per hour, (d) number of mixed-frequency events per hour, (e) $\log_{10}$ energy release of mixed-frequency events per hour, and (f) volume strain tide. Horizontal bars show segments of time series selected for correlation estimates given in Table 2 and Figure 8; the sign of the slope of the linear regression line (plus or minus) and the confidence level of the regression (percent) are shown beneath each bar. The regressions are calculated with strain rate in the first and third intervals, with strain in the second. Note that the changes in phase of the correlations occur near the time of volcanic tremor onset (March 31) and near the time of decrease in overall seismic energy release rate (April 3; see Figure 3).

earth strain tides are calculated by Longman's [1959] method by using a well-tested program. Ocean load tides are calculated from the tidal models of Schwiderski [1980, 1982] and the Green's functions of Farrell [1972] for four semidiurnal, four diurnal, and one long-period constituents using elastic constants $\lambda = 3.42 \times 10^{10}$ Nm^{-2}, $\mu = 3.45 \times 10^{10}$ Nm^{-2} in the crust; these are added to the solid earth tides. The Schwiderski data are tabulated on a 1° x 1° grid over the open ocean, and the grid is used directly for calculating stresses and strains due to loading by ocean tides located more than 500 km away from Mount St. Helens. Closer than this, the grid is interpolated onto a finer mesh, including an accurate representation of the coastline within 300 km of the volcano. The magnitude of the combined open ocean and coastal load tides is typically 20-40% that of the solid earth tides for linear strain components at the location of Mount St. Helens; hence their neglect could significantly affect the results. For studies of tidal triggering of earthquakes in areas located closer to the coast than Mount St. Helens (≈130 km) the ocean load effect could be even greater. For the volume strain tides used in our correlation statistics, the magnitude of the ocean load tides is about 10% that of the solid earth tides.

The earthquake data consist of eight time series from station CPW; four are the number of earthquakes per hour in each class, and four are the values for $\log_{10}$ of the energy release (Figures 5b and 5c). We examine each time series before, during, and after each of the time periods discussed above to determine if there is any statistically significant tidal correlation. We also divide the time series arbitrarily into equal 4-day segments and test these for tidal correlation.

We employ linear regression statistics on each record segment to search for a linear relationship, first between number of earthquakes per hour and tidal strain amplitude, then between number of quakes per hour and tidal strain rate. We then perform the same calculations by using $\log_{10}$ (energy release) per hour. Our calculations use the volume strain tide (Figure 5a), which is directly proportional to volume stress or pressure.

Computed correlation coefficients vary between 0 and 0.4. Out of the total of 160 regressions performed between the tides and number of earthquakes per hour (104 on random 4-day segments, 56 on specially chosen segments), 12 were significant at the 95% confidence level, somewhat higher than would be expected by chance. Furthermore, 7 of these were for just the low- and mixed-fre-

quency events during the 10-day period March 27 to April 5, 1980. The remaining high correlations were distributed randomly in time and between different classes of earthquakes, hence we do not consider them significant. The March 27 to April 5 portions of the time series are displayed at enlarged scale in Figure 7, in which it is possible to identify three distinct periods of correlation. Figure 8a shows scatter plots for these periods with the best fit linear regression line plotted. We have also performed an alternative test of correlation with semidiurnal tidal phase, using Schuster's test as described by Klein [1976]. The test is performed by dividing the time between successive semidiurnal tidal peaks into 12 equal intervals and assigning quakes to these intervals depending on their time of occurrence. The numbers of earthquakes per interval are plotted as rose diagrams in Figure 8b. The quakes are added vectorially with unit magnitude for each quake, and a phase depending on the elapsed time since the previous semidiurnal peak. The larger the magnitude of the resulting vector, the less likely that the earthquake distribution could have occurred by chance; the direction of the resultant gives the most probable time of earthquake occurrence relative to semidiurnal high tide. This procedure assumes for its validity that the semidiurnal tide is dominant at the site in question; the tidal time series displayed in Figure 7 demonstrate that this assumption is justified. Results of both types of test are given in Table 2. Though we believe the linear-regression tests using accurately calculated synthetic stress or strain tides are more useful in that they can give some insight into the mechanism of the earthquake-tide correlation, it is of interest that the Schuster test gives comparable, though not identical, results.

During the time period in which the correlations occur, the smaller events were predominant in the low- and mixed-frequency event classes (Figure 6). Since the events were therefore all of roughly the same energy, this explains why the correlations are similar for both number of earthquakes and for energy. The phase of the correlation of the low-frequency events is exactly opposite that of the mixed-frequency events for the first two time intervals when both classes show correlation with the tides. Also, the phase of the correlation varies systematically between the three time intervals. The low-frequency events correlate with positive strain rate in the first interval, with negative strain in the second, and with negative strain rate in the third (Figures 7 and 8a). These variations appear as systematic changes in orientation of the resultant vector in the rose diagrams (Figure 8b). The physical significance of the correlations and phase changes are discussed below. However, several points should be made here. First, the correlations are rather weak, amounting to a difference of only two or three earthquakes per hour between different parts of the tidal cycle. Second, since the low- and mixed-frequency correlations have opposite sign, it is possible that the correlations would disappear if the two classes of events were combined. In fact they do not, since the slopes of the regressions are different for the two classes; in any case, the two classes of events are quite distinct on the seismograms (Figure 4) and events were assigned to each class independently of any knowledge of the tides, so we believe recombination of the two classes is unjustified. Third, it is possible that the progressive advance of the phase of the correlation with respect to the semidiurnal tide could be explained if the correlation were not with the tide at all, but with a half daily (i.e., 12 hours rather than ≈12 hours 25 min) period (though we have no suggestion for what the mechanism might be). If this were the case, a Schuster test using a 12 hour sine wave as the "tidal" series would give the same azimuth of resultant for each of the three time intervals. The results in Table 2 argue against this possibility. The correlations with the 12-hour sine wave are good, as would be expected, but the phase (e.g., 113°, 99°, 17° for the low-frequency events) is not constant. Fourth, it is noticeable both in Figures 7 and 8a that the correlations are controlled as much by the hours in which no earthquakes occur as by those in which large numbers occur. It is thus possible that the tides act to inhibit earthquake occurrence during one part of the tidal cycle rather than by enhancing it during the opposite part. Finally, though the concentration of significant tidal correlations for the low- and mixed-frequency events into a 10 day time period is suggestive, and though the phase of the correlations appears to vary systematically, the correlations only persist for a few tidal cycles each. Hence while the formally estimated confidence levels are high, it is possible, though we think unlikely, that the correlations are spurious.

Discussion and Conclusions

Since the Pavlof results [McNutt and Beavan, 1981] indicated that a tidal correlation appeared approximately 4 days before the onset of periods of explosive eruptive activity, we felt that the tidal analysis described above might offer some predictive capability, when carefully combined with other techniques.

However, Pavlof and Mount St. Helens have quite different seismic and eruptive characteristics. We present here a comparison of the two volcanoes, since there is no a priori reason to suspect their behavior with respect to tidal stresses should be the same. At Pavlof, low-frequency emergent events with no clear S phases (Minakami's [1960] B-type events) take place at the rate of several tens per day during background periods; numbers increase to several hundred events per day prior to and during explosive eruptions. Magnitudes for these B-type events are all less than about 1.0. Virtually no A-type events (those events with clear P and S phases and depths of 1-10 km [Minakami, 1960]) have been recorded at Pavlof from 1973 to 1983; only four such events large enough to locate have occurred within 15 km of the volcano during 10 years of recording. Pavlof's eruptions consist of lava fountaining from a small summit vent, and numerous small Strombolian explosions (as many as 13 per hour have been recorded). Six large eruptions have occurred in the 10 years of seismic recording; basalt with about 52% SiO_2 is the

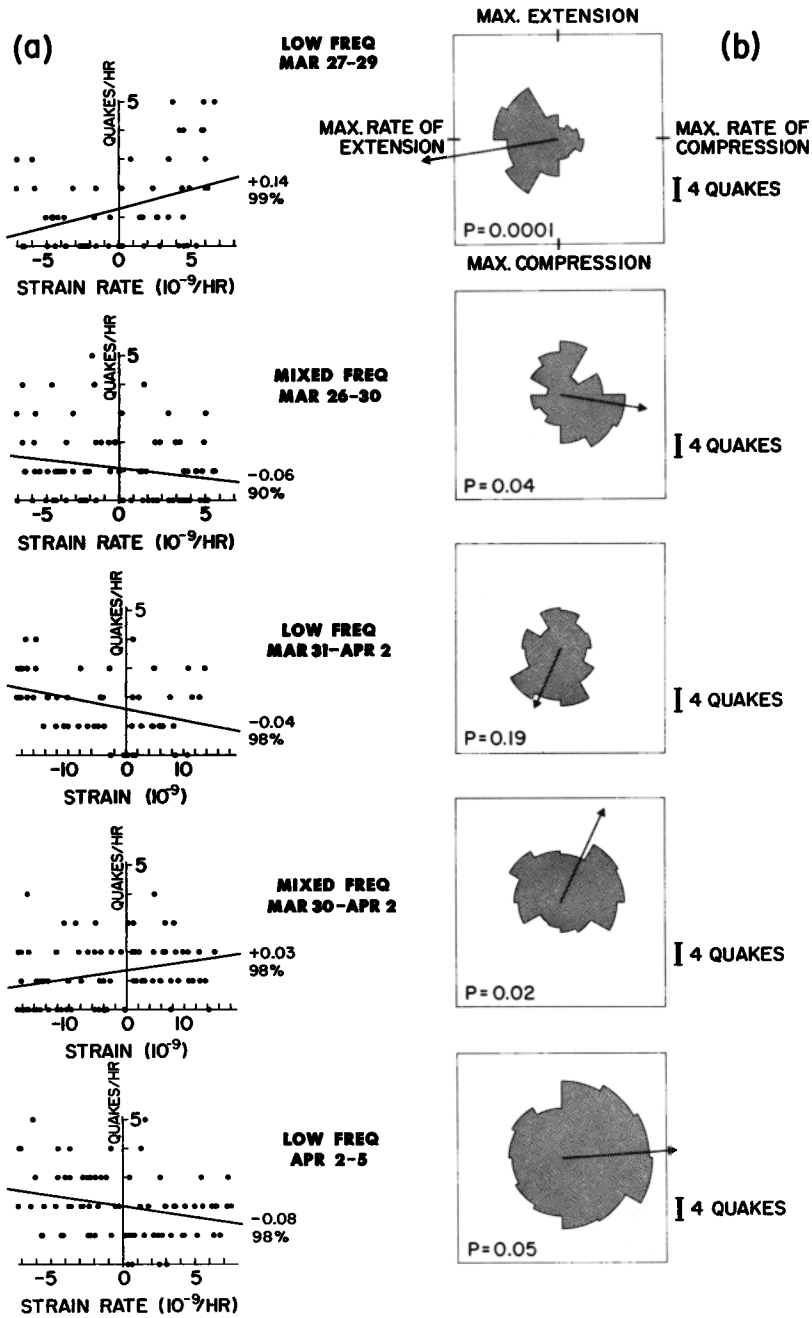

Fig. 8. (a) Scatter plots between number of earthquakes per hour and strain or strain rate for the time series segments shown in Figure 7. The best fit linear regression line is shown with its slope and confidence level. Note that the slope of the regression is opposite for the low- and mixed-frequency earthquakes during a particular time period. Also, the correlation changes with time. For instance, the low-frequency events correlate first with positive strain rate, then with negative strain, then with negative strain rate. (b) Rose diagrams (see text) for the same data. The direction of the resultant vector gives the most likely time of occurrence of earthquakes in the semidiurnal tidal cycle, where the top of the diagram represents maximum extensional tidal strain, the right hand side the maximum rate of compression, the bottom represents maximum compression, and the left represents maximum rate of extension. The value of P is the probability that the length of the resultant vector could be exceeded if earthquakes occur randomly in time. Thus (1 - P) x 100 is a statistic comparable to the linear regression confidence level. Note that the resultants are in opposite directions for low- and mixed-frequency events during a particular time segment, and that they both change systematically by ≈90° from one time segment to the next.

TABLE 2. Observed Correlations Between Earthquakes and Tides

	Regression							Schuster Test				
	Number of Events per Hour			Log_{10} (Energy Release per Hour)					Strain		12-Hour Sine Wave	
	r	s	c	r	s	c	T	N	P	ϕ	P	ϕ
				Low Frequency								
Mar. 27-29 Strain rate	0.40	0.14	99	0.31	0.05	98	58	79	0.0001	- 99	0.0003	113
Mar. 31 to Apr. 2 Strain	0.35	-0.04	98	0.37	-0.02	99	53	89	0.18	-156	0.28	99
Apr. 2-5 Strain rate	0.29	-0.08	98	0.20	-0.02	90	76	154	0.05	86	0.07	17
				Mixed Frequency								
Mar. 26-30 Strain rate	0.20	-0.06	90	0.19	-0.03	90	81	89	0.04	100	0.06	-59
Mar. 30 to Apr. 3 Strain	0.27	0.03	98	0.32	0.03	99	83	105	0.02	25	0.007	-80

Here r is correlation coefficient, s is slope of regression line in number of events per hour per 10^{-9} strain, or in $\log_{10}$(energy release in ergs) per hour per strain rate of 10^{-9}/hour, c is confidence level in percent, T is number of hours data used in the regressions, N is number of earthquakes occurring within time interval, P is probability that resultant vector (Figure 8b) would be so large by chance, and ϕ is phase of resultant in degrees relative to the preceding semidiurnal maximum extensional strain.

most common lava. These data suggest that Pavlof has a relatively open plumbing system, which does not permit the buildup of large stresses. Mount St. Helens, on the other hand, had earthquakes of several different types and with sizes up to magnitude 5.1 M_L. No eruptions had occurred since the 1850's, and the presence of several dacite domes demonstrates that some older vents had been effectively capped. Further, geological investigations [Crandell and Mullineaux, 1978] have shown that Mount St. Helens has had several large explosive eruptions in the past several thousand years. Thus we contrast the frequent small eruptions of basalt and small earthquakes at Pavlof with Mount St. Helens, which has had larger, less frequent, and more explosive eruptions of dacite, and earthquakes up to 4 orders of magnitude larger. McNutt and Beavan [1981] concluded that eruption processes built up slowly and continuously at Pavlof and that the presumed stress drops of the small, emergent B-type events were small compared to earth tidal stresses (about 0.02 bar); thus Pavlof's volcanic system is more conducive to interaction with the earth tides. At Mount St. Helens, on the other hand, eruption processes build up and change quickly, the earthquakes are large, of different character, and probably have quite variable stress drops which are large relative to tidal stresses. Further, the growth of the Mount St. Helens cryptodome (bulge) alone added about 1 bar per day to the overburden pressure (S. Malone, personal communication, 1980).

Our results show that the pattern of stress release at Mount St. Helens prior to May 18, 1980, was for the most part too rapid and variable to be significantly affected by the earth tides. The only time interval which did show statistically significant tidal correlations was the time period just before and during the first period of volcanic tremor in early April 1980, during which time the cumulative earthquake energy release rate decreased. The earthquakes which showed correlations were of relatively small magnitude. We tentatively interpret the changes in seismic activity as indicators of changing magma movement in the shallow crust beneath the volcano. In particular, the onset of tremor coincided roughly with the beginning of growth of the bulge or cryptodome [Malone et al., 1981; Krimmel and Post, 1981] signaling the arrival of magma near the surface. We conclude that during this stage of activity the volcano was sensitive to small changes in the ambient stress field. We infer that both the low- and mixed-frequency earthquakes occur in response to changes in the local stress field as magma pressure varies. The low- and mixed-frequency events must have different focal mechanisms as they respond to the tide with opposite polarity. However, the systematic and similar changes in the phase of correlation for each class of event suggest that they are also related to each other, whereas the high- and medium-frequency events do not demonstrate any such interdependence. Rather, their patterns of occurrence, as discussed earlier, reveal a simpler mode of stress release. Focal mechanisms for the low- and mixed-frequency events have not been published and were not determined in the present study.

Tidal correlations did not precede the major eruption on May 18, 1980. However, S. Malone (personal communication, 1982) reports that some of the later, smaller eruptions may show tidal periodicities in seismicity and other phenomena similar to those observed at Pavlof; these are not addressed in the present study.

We conclude that while tidal stresses may affect certain stages of volcanic activity, and tidal analyses may be of some utility in predicting small eruptions, they are ineffective in predicting the timing of large eruptions that follow rapid magma buildup such as the catastrophic blast of May 18, 1980, at Mount St. Helens. We feel that further analysis of some of the other seismicity patterns elucidated here, especially those for the low-frequency events, which seem to occur only at volcanos, offers potential for development of quantitative seismic methods of forecasting major volcanic eruptions.

Acknowledgments. Members of the Geophysics Program, University of Washington, were very helpful in providing logistical support and insightful comments regarding the data. We especially appreciate their help during times when working conditions were quite strained. In particular, we thank E. Endo, R. Crosson, S. Malone, C. Weaver, L. Noson, J. Booker, S. Smith, D. Leaver, W. Grant, C. Boyko, C. Michaelson, and R. Norris. Special thanks to the Nadreaus for their generous hospitality (S.R.M.). The manuscript was critically reviewed by K. Jacob and T. Engelder. This work was supported by the National Science Foundation (grant EAR 80-24006) and the Department of Energy (DE-AC02-76ER03134). Lamont-Doherty Geological Observatory contribution 3604.

References

Crandell, D. R., and D. Mullineaux, Potential hazards from future eruptions of Mount St. Helens Volcano, Washington, U.S. Geol. Surv. Bull., 1383-C, 26 pp., 1978.

Decker, R., and B. Decker, The eruptions of Mount St. Helens, Sci. Am., 244, 68-80, 1981.

Endo, E. T., S. D. Malone, L. L. Noson, and C. tics of the March 20-May 8 earthquake sequence, The 1980 Eruptions of Mount St. Helens, Washington, edited by P. W. Lipman and D. R. Mullineaux, U.S. Geol. Surv. Prof. Pap., 1250, 93-107, 1981.

Farrell, W. E., Deformation of the earth by surface loads, Rev. Geophys. Space Phys., 10, 761-797, 1972.

Geophysics Program, University of Washington, Eruption of Mount St. Helens: Seismology, Nature, 285, 529-531, 1980.

Gutenberg, B., and C. F. Richter, Seismicity of the Earth and Associated Phenomena, 273 pp., Princeton University Press, Princeton, N. J., 1954.

Klein, F. W., Earthquake swarms and the semidiurnal solid earth tide, Geophys. J. R. Astron. Soc., 45, 245-295, 1976.

Krimmel, R. M., and A. Post, Oblique aerial photography, March-October 1980, The 1980 Eruptions of Mount St. Helens, Washington, edited by P. W. Lipman and D. R. Mullineaux, U.S. Geol. Surv. Prof. Pap., 1250, 31-52, 1981.

Lipman, P. W., J. G. Moore, and D. A. Swanson,

Bulging of the north flank before the May 18 eruption--Geodetic data, The 1980 Eruptions of Mount St. Helens, Washington, edited by P. W. Lipman and D. R. Mullineaux, U.S. Geol. Surv. Prof. Pap., 1250, 143-156, 1981.

Longman, I. M., Formulas for computing the tidal accelerations due to the moon and the sun, J. Geophys. Res., 64, 2351-2355, 1959.

Malone, D. S., E. T. Endo, C. S. Weaver, and J. W. Ramey, Seismic monitoring for eruption prediction, The 1980 Eruptions of Mount St. Helens, Washington, edited by P. W. Lipman and D. R. Mullineaux, U.S. Geol. Surv. Prof. Pap., 1250, 803-813, 1981.

McNutt, S., Preliminary calculations of Mount St. Helens b-values (abstract), Eos Trans. AGU, 62, p. 62, 1981.

McNutt, S. R., and R. J. Beavan, Volcanic earthquakes at Pavlof volcano correlated with the solid earth tide, Nature, 294, 615-618, 1981.

Minakami, T., Fundamental research for predicting volcanic eruptions, I, Earthquakes and crustal deformations originating from volcanic activities, Bull. Earth Res. Inst. Tokyo Univ., 38, 497-544, 1960.

Noson, L. L., and R. S. Crosson, Correlation of earthquake hypocenters in western Washington--1978, Wash. State Dep. Nat. Resour. Inf. Circ., 72, 18 pp., 1980.

Page, R., Aftershocks and microaftershocks of the great Alaska earthquake of 1964, Bull. Seismol. Soc. Am., 58, 1131-1168, 1968.

Richter, C. F., Elementary Seismology, 768 pp., W. H. Freeman, San Francisco, Calif., 1958.

Schwiderski, E. W., On charting global ocean tides, Rev. Geophys. Space Phys., 18, 243-268, 1980.

Schwiderski, E. W., Global ocean tides, X, Report NSWC TR 82-151, Nav. Surface Weapons Cent., Dahlgren, Va., 1982.

Utsu, T., A method for determining the value of b in a formula log n = a - bM showing the magnitude-frequency relation for earthquakes, Geophys. Bull. Hokkaido Univ., 13, 99-103, 1965.

S. R. McNutt and R. J. Beavan, Lamont-Doherty Geological Observatory of Columbia University, Palisades, NY 10964.

(Received May 31, 1983;
revised January 27, 1984;
accepted January 27, 1984.)